

**Multistability of electromagnetically induced transparency in atom-assisted optomechanical cavities**Yue Chang,<sup>1</sup> T. Shi,<sup>1</sup> Yu-xi Liu,<sup>2,3,4</sup> C. P. Sun,<sup>1</sup> and Franco Nori<sup>2,3,5</sup><sup>1</sup>*Institute of Theoretical Physics, Chinese Academy of Sciences, Beijing 100190, China*<sup>2</sup>*Advanced Science Institute, The Institute of Physical and Chemical Research (RIKEN), Wako-shi 351-0198, Japan*<sup>3</sup>*CREST, Japan Science and Technology Agency (JST), Kawaguchi, Saitama 332-0012, Japan*<sup>4</sup>*Institute of Microelectronics, Tsinghua National Laboratory for Information Science and Technology (TNList), Tsinghua University, Beijing 100084, China*<sup>5</sup>*Center for Theoretical Physics, Physics Department, Center for the Study of Complex Systems, The University of Michigan, Ann Arbor, Michigan 48109-1040, USA*

(Received 25 May 2009; published 22 June 2011)

We study how an oscillating mirror affects the electromagnetically induced transparency (EIT) of an atomic ensemble confined in a gas cell, which is placed inside a microcavity with an oscillating mirror in one end. The cavity field acts as a probe of the EIT system and also produces a light pressure on the mirror. The back-action from the mirror to the cavity field results in several (from one to five) steady-states for this atom-assisted optomechanical cavity, producing a complex structure in its EIT. The multiequilibrium positions of the oscillating mirror have been calculated, and then the susceptibility is studied with respect to the different equilibrium positions. We find that the EIT of the atomic ensemble can be significantly changed by the oscillating mirror, and also the various steady states of the mirror have different effects on the EIT.

DOI: [10.1103/PhysRevA.83.063826](https://doi.org/10.1103/PhysRevA.83.063826)

PACS number(s): 42.50.Gy, 42.50.Pq, 32.80.Qk

**I. INTRODUCTION**

Fast developments are now occurring in studies at the interface between different kinds of physical systems. Examples of these include: couplings between light and nano- or micromechanical systems (e.g., in Refs. [1–10]), called optomechanical systems; interactions between superconducting artificial atoms (e.g., charge or flux qubit); and transmission line resonators (e.g., in Refs. [11–16]); and so on. These studies are partly motivated by possible physical implementations of quantum information processing, to explore potential future devices, and to study the interesting physics in these hybrid structures.

In optomechanical systems (e.g., in Refs. [1–10]), the radiation pressure acts on the oscillating mirror and induces the interaction between the mechanical system and the optical field. The back-action from the mirror to the cavity field [17] can result in several steady-state solutions for the equilibrium position of the mirror, e.g., it has been proved [1] that this system experiences bistability in some parameter region. It has also been shown that light pressure can be used to realize entanglement between the cavity field and a microscopic object (e.g., a movable mirror) [1–4], and can also cool down the mirror [5–8]. Furthermore, Refs. [18,19] studied optomechanical cavities containing a two-level atomic ensemble. The atomic ensemble effectively enhances the radiation pressure of the cavity field on the oscillating mirror, producing a cavity-atom-mirror entanglement [18,19]. In this paper we consider this atom-optical system with a three-level atomic ensemble, which can enable quantum interference, e.g., electromagnetically induced transparency.

Electromagnetically induced transparency (EIT) is a remarkable quantum interference phenomenon, which enables the active control of light propagation in a coherent medium [20–23]. Usually, the basic population transfer configuration for the atoms in EIT is of  $\Lambda$  type, where the two transitions from a common upper energy level to two lower energy levels are induced by two different optical fields (e.g., classical control

field and quantized probe field) [24–26], respectively. One is a strong field, and the other is a weak one. The stronger field can effectively modify the susceptibility of the medium so that the weak one (as a probe signal) can pass through the medium transparently at the two-photon resonance [27–31]. Recently, it has been shown that this effect can also work well at the single photon level for the probe light [32], and thus the weak field must be treated quantum mechanically. In the quantum approach, a dark state with dressed photons can be invoked to store quantum information of photons on the atomic ensemble as quantum memory [33,34]. These quantum manipulations at the single photon level require frequency matching with extremely high precision for one- or two-photon resonance. When the quantum field is provided by a microcavity with a one-end oscillating mirror, the oscillation of the mirror might affect such a precise frequency-matching condition and thus affect the EIT.

Motivated by these works, here we study how the oscillating mirror changes the properties of the EIT. We will study the atom-assisted optomechanical microcavity, through which we explore the possibility to interface other systems, via some physical mechanism, such as EIT. Here, the three-level atomic ensemble for each atom with  $\Lambda$ -type transitions is placed inside a cavity with a one-end oscillating mirror. Due to the mirror's oscillation, the susceptibility of this atomic medium displays a multistability corresponding to the multiequilibrium positions of the mirror. Another prediction of our study is that the mirror's oscillation significantly alters the properties of both the real and imaginary parts of the susceptibility, and thus makes the EIT phenomena change. We also investigate in detail how the different steady states of the mirror influence the dispersion relations and absorption properties of the light.

The paper is organized as follows. In Sec. II, we introduce the model for the optomechanical system with the EIT. In Sec. III, we present the Heisenberg-Langevin equations for

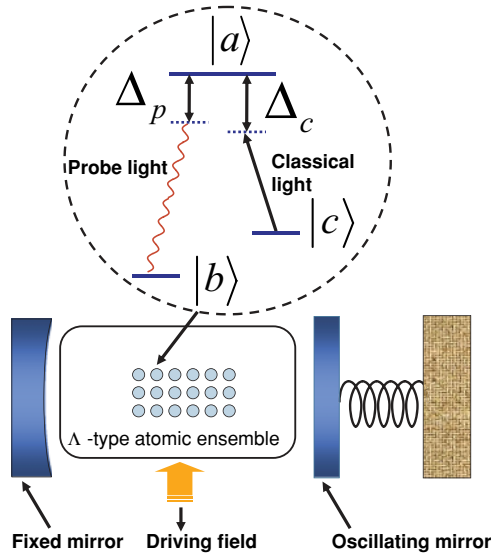


FIG. 1. (Color online) Schematic diagram for the atom-assisted optomechanical system considered here. There are three main components: (i) an optical cavity with one fixed mirror; (ii) another oscillating mirror, which is modeled as a quantum-mechanical harmonic oscillator (denoted by a black spring); and (iii) an ensemble of identical three-level atoms, which are confined inside the cavity. Each atom is assumed to have  $\Lambda$ -type transitions. Here,  $\Delta_p = \omega_a - \omega_0 + \omega_0(x)/l$  and  $\Delta_c = \omega_a - \omega_c - \nu$ .

this system and obtain several (from one to five, depending on the system parameters) steady-state solutions for the position of the oscillating mirror. In Sec. IV, we study the EIT with susceptibilities for different (from one to two) equilibrium positions of the mirror. In Sec. V, we summarize our results.

## II. ATOM-ASSISTED OPTOMECHANICAL SYSTEM

As shown in Fig. 1, we consider an ensemble of  $N$  identical three-level atoms, which are confined inside an optical cavity with a one-end oscillating mirror. The excited, metastable, and ground states of the  $i$ th atom are denoted by  $|a\rangle_i$ ,  $|c\rangle_i$ , and  $|b\rangle_i$ . Each atom is assumed to have  $\Lambda$ -type transitions. That is, for the  $i$ th atom, a classical light field with the frequency  $\nu$  induces a transition between  $|a\rangle_i$  and  $|c\rangle_i$ , which is often used as a control field. The quantized cavity field, with the frequency  $\omega_0$  when the oscillating mirror is fixed, induces the transition between  $|a\rangle_i$  and  $|b\rangle_i$ . We assume that this cavity field acts as a probe field. Here, the transition between  $|b\rangle_i$  and  $|c\rangle_i$  is assumed to be forbidden. The oscillating mirror is modeled as a quantum-mechanical harmonic oscillator with the frequency  $\omega_M$  and the mass  $M$ . This harmonic oscillator can also be considered as a spring with an elastic coefficient  $M\omega_M^2$ .

Based on the above considerations, and using  $\hbar = 1$ , the Hamiltonian of the total system

$$H = H_C + H_M + H_A + H_{M-C} + H_{A-L} \quad (1)$$

has five terms corresponding to (i) the cavity ( $H_C$ ), (ii) the oscillating mirror ( $H_M$ ) of the mass  $M$ , (iii) the atom gas ( $H_A$ ), (iv) the mirror cavity ( $H_{M-C}$ ), and (v) the atom-light term ( $H_{A-L}$ ). Explicitly, these are described below:

(i) the free Hamiltonian

$$H_C = \omega_0 a^\dagger a, \quad (2)$$

of the single-mode cavity field with the annihilation and creation operators  $a$  and  $a^\dagger$ ; this term (and  $\omega_0$ ) refers to a cavity with two fixed mirrors;

(ii) the free Hamiltonian

$$H_M = \frac{p^2}{2M} + \frac{1}{2} M \omega_M^2 x^2, \quad (3)$$

of the oscillating mirror, where  $p$  is the momentum of the oscillating mirror with a small displacement  $x$ ;

(iii) the free Hamiltonian

$$H_A = \sum_{i=1}^N (\omega_a \sigma_{aa}^{(i)} + \omega_c \sigma_{cc}^{(i)}), \quad (4)$$

of the  $N$  three-level  $\Lambda$  atoms with the operators  $\sigma_{\alpha\alpha}^{(i)} = |\alpha\rangle_i \langle\alpha|$  and  $\alpha = a, c$ ; here,  $\omega_a$  ( $\omega_c$ ) is the energy-level spacing between  $|a\rangle_i$  and  $|b\rangle_i$  ( $|c\rangle_i$  and  $|b\rangle_i$ ) for the  $i$ th atom, and we have assumed the ground state  $|b\rangle_i$  as an energy reference point;

(iv) the interaction Hamiltonian

$$H_{M-C} = -\frac{\omega_0}{l} x a^\dagger a, \quad (5)$$

between the cavity field and the oscillating mirror [1], presents a radiation pressure on the mirror due to the small change  $x$  of the cavity length when the mirror oscillates [5], where  $l$  is the cavity length when the mirror is fixed;

(v) the interaction Hamiltonian

$$H_{A-L} = \sum_{i=1}^N (\Omega e^{-i\nu t} \sigma_{ac}^{(i)} + g a \sigma_{ab}^{(i)} + \text{H.c.}), \quad (6)$$

between the three-level atoms and the classical as well as the quantized fields. In Eq. (6),  $\Omega$  is the Rabi frequency associated with the coupling between the classical field and the three-level atoms. The frequency  $\nu$  is assumed to satisfy the condition

$$\nu = \omega_a - \omega_c - \Delta_c. \quad (7)$$

Here,  $\Delta_c$  is the detuning between the frequency of the classical control field and the transition frequency from the energy level  $|a\rangle_i$  to the energy level  $|c\rangle_i$  for the  $i$ th atom. The parameter

$$g = -\mu \sqrt{\omega_0 / 2V \epsilon_0} \quad (8)$$

in (6) describes the coupling between the quantized cavity field and the three-level atoms, where  $\mu$  is the electric-dipole transition matrix element between levels  $|a\rangle_i$  and  $|b\rangle_i$ ,  $V$  describes the volume of the cavity, and  $\epsilon_0$  is the permittivity of the vacuum. We note that the effect of the oscillating mirror on the coupling between the atoms and the quantized cavity field [35] has been neglected when the Hamiltonian in Eq. (1) was derived, because we do not consider the strong coupling between the quantized field and the atoms.

The dynamics of the system governed by the Hamiltonian  $H$  in Eq. (1) is depicted by the Heisenberg-Langevin equations

$$\partial_t x = \frac{p}{M}, \quad (9a)$$

$$\partial_t p = -\frac{\gamma_M}{2M} p + \frac{\omega_0}{l} a^\dagger a - M \omega_M^2 x - \sqrt{\gamma_M} \epsilon_{\text{in}}(t), \quad (9b)$$

$$\partial_t a = -\frac{\gamma_0}{2} a - i\omega_0 \left(1 - \frac{x}{l}\right) a - ig \sum_{i=1}^N \sigma_{ba}^{(i)} + \sqrt{\gamma_0} a_{\text{in}}(t), \quad (9c)$$

$$\begin{aligned} \partial_t \sum_{i=1}^N \sigma_{ba}^{(i)} = & -(\gamma_1 + i\omega_a) \sum_{i=1}^N \sigma_{ba}^{(i)} - i\Omega e^{-i\omega t} \sum_{i=1}^N \sigma_{bc}^{(i)} \\ & - ig a \sum_{j=1}^N [\sigma_{bb}^{(j)} - \sigma_{aa}^{(j)}] + \sqrt{N} f_1(t), \end{aligned} \quad (9d)$$

$$\begin{aligned} \partial_t \sum_{i=1}^N \sigma_{bc}^{(i)} = & -\gamma_2 \sum_{i=1}^N \sigma_{bc}^{(i)} - i\omega_c \sum_{i=1}^N \sigma_{bc}^{(i)} - i\Omega e^{i\omega t} \sum_{i=1}^N \sigma_{ba}^{(i)} \\ & + ig a \sum_{j=1}^N \sigma_{ac}^{(j)} + \sqrt{N} f_2(t). \end{aligned} \quad (9e)$$

Here, for convenience, we have neglected detailed derivations as in Ref. [24], and just phenomenologically introduce the damping  $\gamma_M$  of the oscillating mirror, the decay rates  $\gamma_0$  for the cavity field, and the decay rate  $\gamma_1$  ( $\gamma_2$ ) from  $|a\rangle$  to  $|b\rangle$  ( $|c\rangle$  to  $|b\rangle$ ). The decay from  $|c\rangle$  to  $|b\rangle$  is an equivalent result although there is no direct electric dipole transition between the energy levels  $|c\rangle$  and  $|b\rangle$ . Physically, this decay is from the electric dipole transitions between  $|a\rangle$  and  $|b\rangle$  as well as  $|a\rangle$  and  $|c\rangle$ , which can be referred to Ref. [24]. We also assume that the quantum fluctuations of the cavity field, mirror, and the atoms satisfy the conditions

$$\langle \epsilon_{\text{in}}(t) \rangle = \langle f_1(t) \rangle = \langle f_2(t) \rangle = 0 \quad (10)$$

and

$$\langle a_{\text{in}}(t) \rangle = \alpha_{\text{in}}(t). \quad (11)$$

Here,  $\alpha_{\text{in}}(t)$  can be understood as an input driving field. That is,  $a_{\text{in}}(t)$  can be rewritten as

$$a_{\text{in}}(t) = \alpha_{\text{in}}(t) + \delta a_{\text{in}}(t), \quad (12)$$

where the quantum fluctuation of the input field  $\delta a_{\text{in}}(t)$  satisfies  $\langle \delta a_{\text{in}}(t) \rangle = 0$ .

### III. HEISENBERG-LANGEVIN EQUATIONS AND MULTISTABILITY

#### A. Steady-state positions of the movable mirror: Analytical results

We are interested in the steady-state solutions. In the derivation of the Hamiltonian in Eq. (1), we have assumed that the linear size of the atomic ensemble is much smaller than the wavelengths of the light fields. In this case, the couplings between the atoms and the light fields are homogeneous, and we can define the collective operators of the atomic ensemble as in Refs. [25,30]:

$$S = \sum_{i=1}^N \sigma_{aa}^{(i)}, \quad A^\dagger = \frac{1}{\sqrt{N}} \sum_{i=1}^N \sigma_{ab}^{(i)}, \quad (13a)$$

$$T_+ = (T_-)^\dagger = \sum_{i=1}^N \sigma_{ac}^{(i)}, \quad C = \frac{1}{\sqrt{N}} \sum_{i=1}^N \sigma_{bc}^{(i)}. \quad (13b)$$

Together with Eqs. (13a) and (13b), the interaction Hamiltonian  $H_{A-C}$  in Eq. (6) can be rewritten as

$$H_{A-L} = \Omega e^{-i\omega t} T_+ + g\sqrt{N} a A^\dagger + \text{H.c.} \quad (14)$$

by using the collective operators.

Let us now assume: (i) the number  $N$  of atoms is large enough; (ii) most of the atoms are in the ground state, i.e., the atomic system is in very low excitation. Based on these two assumptions, we can find that the collective operators in Eqs. (13a) and (13b) satisfy the commutation relations as in Refs. [19,25,30]:

$$[C^\dagger, S] = 0, \quad [A, S] = A, \quad (15a)$$

$$[T_-, C^\dagger] = 0, \quad [T_+, C^\dagger] = A^\dagger, \quad (15b)$$

$$[A, C] = 0, \quad [T_+, A] = -C, \quad (15c)$$

$$[T_-, C] = -A, \quad (15d)$$

$$[A, C^\dagger] = \frac{1}{N} T_- \approx 0, \quad (15e)$$

$$[A, A^\dagger] = \frac{1}{N} \sum_{j=1}^N [\sigma_{bb}^{(j)} - \sigma_{aa}^{(j)}] \approx 1, \quad (15f)$$

$$[C, C^\dagger] = \frac{1}{N} \sum_{j=1}^N [\sigma_{bb}^{(j)} - \sigma_{cc}^{(j)}] \approx 1. \quad (15g)$$

Here, it is clear that  $\sigma_{bb}^{(j)}$ ,  $\sigma_{aa}^{(j)}$  and  $\sigma_{cc}^{(j)}$  are the population operators that the  $i$ th atom is in different states. In the following calculations, we are interested in the average values in the steady states. Based on the assumption that most of the atoms are in the ground state, the average  $\langle \sigma_{bb} \rangle \approx 1$ , but other averages  $\langle \sigma_{cc} \rangle \approx 0$  and  $\langle \sigma_{aa} \rangle \approx 0$ . Thus the averages of collective operators  $\sum_{j=1}^N \sigma_{aa}^{(j)} / \sqrt{N}$  and  $\sum_{j=1}^N \sigma_{cc}^{(j)} / \sqrt{N}$  are much smaller than one due to the low excitation in the excited states  $|a\rangle$  and  $|c\rangle$ , however,  $\sum_{j=1}^N \sigma_{bb}^{(j)} / \sqrt{N}$ ,  $A$  and  $C$  are large quantities due to the large number of atom in the ground state  $|b\rangle$ . Moreover our calculations below are not related to the correlation spectrum, thus the small contributions of the average of the operator  $\sum_{j=1}^N \sigma_{ac}^{(j)} / \sqrt{N}$ , which characterizes the transitions between two upper levels, is neglected below.

Equations (15a) and (15b) present a dynamical symmetry in our system described by the semidirect-product algebra containing the algebra  $SU(2)$  with its generators  $T_\pm$ . It is easy to prove, as in Ref. [19], that the collective operators and the commutation relations can also be given in a similar way as in Eqs. (6), (15a)–(15g) for the case when the couplings between different atoms and the light fields are inhomogeneous. Therefore, our study here can be generalized to the case of inhomogeneous couplings.

Using the commutation relations in Eqs. (15a)–(15g) in the low excitation of the atomic system, the Heisenberg-Langevin equations (9a)–(9e) are now simplified to

$$\partial_t x = \frac{p}{M}, \quad (16a)$$

$$\partial_t p = -\frac{\gamma_M}{2M} p + \frac{\omega_0}{l} a^\dagger a - M\omega_M^2 x - \sqrt{\gamma_M} \epsilon_{\text{in}}(t), \quad (16b)$$

$$-\partial_t a = -\frac{\gamma_0}{2} a - i\omega_0 \left(1 - \frac{x}{l}\right) a - ig\sqrt{N} A + \sqrt{\gamma_0} a_{\text{in}}(t), \quad (16c)$$

$$\partial_t A = -\gamma_1 A - i\omega_a A - i\Omega e^{-i\nu t} C - ig\sqrt{N} a + f_1(t), \quad (16d)$$

$$\partial_t C = -\gamma_2 C - i\omega_c C - i\Omega e^{i\nu t} A + f_2(t). \quad (16e)$$

We note: (i) the equation of motion for the operator  $T_-$  is decoupled from the above equations; (ii) we can also derive the equations of motion without considering the low excitation approximation first, and then we can obtain the same results as the above by taking this approximation when we solve the steady-state equations.

To obtain the steady-state solutions, let us first remove the fast varying factors by the following rotating transformations:

$$a = \tilde{a} \exp(-i\omega_L t), \quad (17a)$$

$$A = \tilde{A} \exp(-i\omega_L t), \quad (17b)$$

$$C = \tilde{C} \exp[i(\Delta_p - \Delta_c - \omega_c)t], \quad (17c)$$

and

$$a_{\text{in}}(t) = \tilde{a}_{\text{in}}(t) \exp(-i\omega_L t) \quad (17d)$$

$$= [\tilde{\alpha}_{\text{in}}(t) + \delta\tilde{\alpha}_{\text{in}}(t)] \exp(-i\omega_L t), \quad (17e)$$

where the detuning  $\Delta_p$  between the transition frequency  $\omega_a$  of the atom, from the energy levels  $|a\rangle$  to  $|b\rangle$ , and the effective frequency  $\omega_L$  of the cavity field, is given by

$$\Delta_p = \omega_a - \omega_L, \quad (18)$$

with the effective cavity frequency

$$\omega_L = \omega_0 - \frac{\omega_0}{l} \langle x \rangle. \quad (19)$$

Here,  $\langle x \rangle$  denotes the mean value of  $x$ . Equation (19) shows that the effective frequency  $\omega_L$  of the cavity can be changed by the oscillating mirror.

In the rotating frame, the Heisenberg-Langevin equations in Eqs. (16b)–(16e) become

$$\partial_t p = -\frac{\gamma_M}{2M} p + \frac{\omega_0}{l} \tilde{a}^\dagger \tilde{a} - M\omega_M^2 x - \sqrt{\gamma_M} \epsilon_{\text{in}}(t), \quad (20a)$$

$$\partial_t \tilde{A} = -(\gamma_1 + i\Delta_p) \tilde{A} - i\Omega \tilde{C} - ig\sqrt{N} \tilde{a} + \tilde{f}_1(t), \quad (20b)$$

$$\partial_t \tilde{C} = -[\gamma_2 + i(\Delta_p - \Delta_c)] \tilde{C} - i\Omega \tilde{A} + \tilde{f}_2(t), \quad (20c)$$

$$\partial_t \tilde{a} = -\left[\frac{\gamma_0}{2} - i\frac{\omega_0}{l}(\langle x \rangle - x)\right] \tilde{a} - ig\sqrt{N} \tilde{A} + \sqrt{\gamma_0} \tilde{a}_{\text{in}}(t), \quad (20d)$$

with the fluctuation

$$\tilde{f}_1(t) = f_1(t) \exp\left[i\omega_0\left(1 + \frac{\langle x \rangle}{l}\right)t\right] \quad (21a)$$

and

$$\tilde{f}_2(t) = f_2(t) \exp[-i(\Delta_p - \Delta_c - \omega_c)t]. \quad (21b)$$

We are interested in the steady-state regime. Let us now assume that all the time derivatives of the mean values for the operators in Eqs. (20a)–(20d) are equal to zero, then we obtain the steady-state equations

$$\frac{\omega_0}{l} \langle \tilde{a}^\dagger \rangle_s \langle \tilde{a} \rangle_s - M\omega_M^2 \langle x \rangle_s = 0, \quad (22a)$$

$$-\frac{\gamma_0}{2} \langle \tilde{a} \rangle_s - ig\sqrt{N} \langle \tilde{A} \rangle_s + \sqrt{\gamma_0} \tilde{\alpha}_{\text{in}} = 0, \quad (22b)$$

$$-(\gamma_1 + i\Delta_{p,s}) \langle \tilde{A} \rangle_s - i\Omega \langle \tilde{C} \rangle_s - ig\sqrt{N} \langle \tilde{a} \rangle_s = 0, \quad (22c)$$

$$-[\gamma_2 + i(\Delta_{p,s} - \Delta_c)] \langle \tilde{C} \rangle_s - i\Omega \langle \tilde{A} \rangle_s = 0. \quad (22d)$$

Here,  $\langle O \rangle_s$  ( $O$  represents the operator in the above steady-state equations) is the mean value of the operator  $O$  under the steady state. The parameter  $\Delta_{p,s}$  is the detuning described in Eq. (18) when the system reaches steady-state. In Eqs. (22a) and (22b), the correlations  $\langle \tilde{a}^\dagger \tilde{a} \rangle_s$  and  $\langle x \tilde{a} \rangle_s$  have been approximately replaced by  $\langle \tilde{a}^\dagger \rangle_s \langle \tilde{a} \rangle_s$  and  $\langle x \rangle_s \langle \tilde{a} \rangle_s$ , respectively. These approximations indicate that the correlations between the fluctuations near the steady states are very small compared to the corresponding mean values in the steady states. This can be quantitatively shown as [36]

$$\frac{\langle (\delta\tilde{a}^\dagger)(\delta\tilde{a}) \rangle_s}{\langle \tilde{a}^\dagger \rangle_s \langle \tilde{a} \rangle_s} \ll 1, \quad \frac{\langle (\delta x)(\delta\tilde{a}) \rangle_s}{\langle x \rangle_s \langle \tilde{a} \rangle_s} \ll 1. \quad (23)$$

From Eqs. (22b)–(22d), when the system reaches the steady-state, the mean values  $\langle \tilde{A} \rangle_s$  and  $\langle \tilde{a} \rangle_s$  can be easily derived as

$$\langle \tilde{A} \rangle_s = \frac{-ig\sqrt{N}\gamma_0 \tilde{\alpha}_{\text{in}} \tilde{\Omega}(\Delta_{p,s})}{G(\Delta_{p,s}) \tilde{\Omega}(\Delta_{p,s}) + \frac{\gamma_0}{2} \Omega^2} \quad (24)$$

and

$$\langle \tilde{a} \rangle_s = \frac{2\tilde{\alpha}_{\text{in}}}{\sqrt{\gamma_0}} \left[ 1 - \frac{g^2 N \tilde{\Omega}(\Delta_{p,s})}{G(\Delta_{p,s}) \tilde{\Omega}(\Delta_{p,s}) + \frac{\gamma_0}{2} \Omega^2} \right], \quad (25)$$

with the functions

$$\tilde{\Omega}(\Delta_{p,s}) = \gamma_2 + i(\Delta_{p,s} - \Delta_c) \quad (26)$$

and

$$G(\Delta_{p,s}) = g^2 N + \frac{1}{2} \gamma_0 (\gamma_1 + i\Delta_{p,s}). \quad (27)$$

Using Eqs. (22a) and (25), we can self-consistently derive a nonlinear implicit equation for  $\Delta_{p,s}$  as below

$$\left| 1 - \frac{g^2 N \tilde{\Omega}(\Delta_{p,s})}{G(\Delta_{p,s}) \tilde{\Omega}(\Delta_{p,s}) + \frac{\gamma_0}{2} \Omega^2} \right|^2 = \frac{\gamma_0 \kappa}{4\tilde{\alpha}_{\text{in}}^2 \omega_0^2} (\Delta_{p,s} - \Delta_0), \quad (28)$$

with the parameters

$$\kappa = M\omega_M^2 l^2, \quad (29)$$

and

$$\Delta_0 = \omega_a - \omega_0. \quad (30)$$

For the detuning  $\Delta_0$  between  $\omega_a$  (the highest frequency of the  $\Lambda$  atom) and  $\omega_0$  [the cavity frequency in Eq. (2) when the two mirrors are fixed]. Equation (28) is a fifth-power implicit equation for  $\Delta_{p,s}$ . Thus the system may have several solutions (i.e., multistability in some parameter regions, corresponding to several steady-state positions of the mirror). These mirror positions are determined by

$$\langle x \rangle_s = \frac{\omega_0 \langle \tilde{a}^\dagger \rangle_s \langle \tilde{a} \rangle_s}{M\omega_M^2 l}. \quad (31)$$

### B. Steady-state positions of the movable mirror: Numerical results

Let us first analyze the atom-cavity detuning  $\Delta_{p,s}$  and the equilibrium positions  $\langle x \rangle_s$  of the mirror. In principle, we can obtain  $\Delta_{p,s}$  by solving the fifth-order equation in Eq. (28). However, instead of this, we obtain  $\Delta_{p,s}$  by plotting the left  $Y_L(\Delta_{p,s})$  and right  $Y_R(\Delta_{p,s})$  hand sides of Eq. (28) as functions of  $\Delta_{p,s}$ , respectively. The real roots of Eq. (28) can be represented by the crossing points of two curves corresponding to  $Y_L(\Delta_{p,s})$  and  $Y_R(\Delta_{p,s})$ . Here, for clarity, these are shown as

$$Y_L(\Delta_{p,s}) = \left| 1 - \frac{g^2 N \tilde{\Omega}(\Delta_{p,s})}{G(\Delta_{p,s}) \tilde{\Omega}(\Delta_{p,s}) + \frac{\gamma_0}{2} \Omega^2} \right|^2, \quad (32)$$

$$Y_R(\Delta_{p,s}) = \frac{\gamma_0 \kappa}{4 \tilde{\alpha}_{\text{in}}^2 \omega_0^2} (\Delta_{p,s} - \Delta_0). \quad (33)$$

The curve and the lines, corresponding to  $Y_L(\Delta_{p,s})$  and  $Y_R(\Delta_{p,s})$ , are schematically shown in Fig. 2, which is used to analyze the solution of the self-consistent equation in Eq. (28). In Fig. 2(a), the double-well-like curve and the straight lines show how  $Y_L(\Delta_{p,s})$  and  $Y_R(\Delta_{p,s})$  changes with  $\Delta_{p,s}$  for a given  $\kappa$  but for larger  $\Delta_0 = \omega_a - \omega_0$ , respectively. Figure 2(b) shows the solution of the self-consistent equation in Eq. (28)

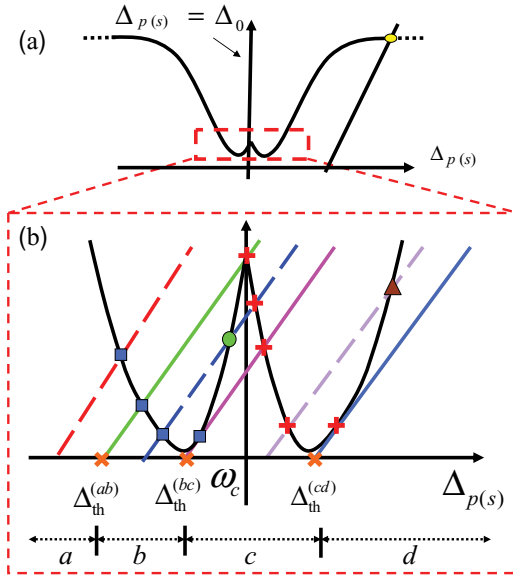


FIG. 2. (Color online) Schematic diagram for the functions of the left  $Y_L(\Delta_{p,s})$  and the right  $Y_R(\Delta_{p,s})$  hand sides of Eq. (28) versus  $\Delta_{p,s}$  in (a) for a large value of  $\Delta_0$  and (b) for  $\Delta_0$  in the region of (a) indicated by the red dashed box. In (b), the brown triangle, red crosses, green dot and blue squares denote four different steady state solutions of the self-consistent equation (28). The brown triangle (far right) denotes the solution  $\Delta_{p,s}^{(1)}$ , the four blue squares (top left) denote the solution  $\Delta_{p,s}^{(2)}$ , the red dots on the curve denotes the solution  $\Delta_{p,s}^{(3)}$ , and the green dot denotes the solution  $\Delta_{p,s}^{(4)}$ . The solution  $\Delta_{p,s}^{(1)}$  is not shown in the regions  $c$  and  $d$ . Here,  $\Delta_{\text{th}}^{(i)}$  ( $i = ab, bc, cd$ ) denote the threshold values of  $\Delta_0$  that separate regions with different number of solutions. Namely,  $\Delta_{\text{th}}^{(ab)}$  is the boundary point of the regions  $a$  and  $b$ ,  $\Delta_{\text{th}}^{(bc)}$  is the boundary point of the regions  $b$  and  $c$ , and  $\Delta_{\text{th}}^{(cd)}$  is the boundary point of the regions  $c$  and  $d$ .

when  $\Delta_0$  is in the region inside Fig. 2(a) marked by the red dashed box.

The slope of the lines in Fig. 2(b) are proportional to  $\kappa$  in Eq. (29). The different straight lines in Fig. 2(b) correspond to different values of  $\Delta_0$ . Recall that  $\Delta_0$  is the atom-cavity detuning when the two mirrors are fixed. Each parameter region for  $\Delta_0$  can have at most five steady-state solutions and three stable solutions. This system has eight parameters. However, during most of this study, we will be varying the atom-cavity detuning  $\Delta_0$  (for fixed mirrors) and the parameter  $\kappa$  as shown in Fig. 2(b). Physically, it is important to study the solution near the atom-cavity detuning  $\Delta_0$ , and the unstable solution shown by the yellow dot in Fig. 2(a) can be neglected.

In the following discussions on the steady-state solutions, we only consider the crossing points between two curves corresponding to  $Y_L(\Delta_{p,s})$  and  $Y_R(\Delta_{p,s})$ , in the red square in Fig. 2(a). Inside this red square, the number of real roots of Eq. (28) can be characterized by three critical values of the detuning  $\Delta_0$ :  $\Delta_{\text{th}}^{(cd)}$ ,  $\Delta_{\text{th}}^{(bc)}$ , and  $\Delta_{\text{th}}^{(ab)}$ , when  $\kappa_L < \kappa < \infty$ . The space of “roots” are divided into four regions presented by the four letters  $a, b, c, d$  at the bottom of Fig. 2(b): (a) when the atom-cavity detuning  $\Delta_0 > \Delta_{\text{th}}^{(cd)}$ , there is no real root; (b) when  $\Delta_{\text{th}}^{(bc)} < \Delta_0 < \Delta_{\text{th}}^{(cd)}$ , there always exist two roots; (c) when  $\Delta_{\text{th}}^{(ab)} < \Delta_0 < \Delta_{\text{th}}^{(bc)}$ , there are four real roots; (d) when  $\Delta_0 < \Delta_{\text{th}}^{(ab)}$ , there are two real roots. Also at the threshold points for  $\Delta_0 = \Delta_{\text{th}}^{(cd)}$ ,  $\Delta_{\text{th}}^{(bc)}$ , and  $\Delta_{\text{th}}^{(ab)}$ , the number of steady-state roots is one, three, and three, respectively. However, in the case when  $\kappa < \kappa_L$ , the threshold value  $\Delta_{\text{th}}^{(ab)}$  does not exist, and there are only two threshold values,  $\Delta_{\text{th}}^{(cd)}$  and  $\Delta_{\text{th}}^{(bc)}$ , which divide the  $\Delta_0$ -parameter space into three regions for the roots of Eq. (28). In this case, the number of roots will be explained below for given sets of parameters.

We now simulate the four steady-state solutions

$$\Delta_{p,s}^{(i)} \equiv \Delta_{\text{probe, steady-state}}^{(\text{particular solution label})}, \quad (i = 1, 2, 3, 4)$$

for given parameters as in Ref. [25], e.g.,  $\Delta_c = 0$ ,  $\omega_a = 10^6$ ,  $\gamma_0 = 10^{-6}$ ,  $\gamma_2 = 10^{-4}$ ,  $g\sqrt{N} = 10^2$ ,  $\Omega = 2$ , and  $a_{\text{in}} = 10$ . Hereafter, all quantities are measured in units of  $\gamma_1$ . With the above parameters, we can find that the lower bound  $\kappa_L$  is about 6400.

We first study the case for  $\kappa < \kappa_L \cong 6400$ , e.g.,  $\kappa = 10^2$ . In this case, there are two critical values  $\Delta_{\text{th}}^{(a)} \cong 25$  and  $\Delta_{\text{th}}^{(b)} \cong -0.95$ . Figure 3 shows the steady-state atom-cavity detunings  $\Delta_{p,s}^{(i)}$  (when the mirror moves) versus  $\Delta_0$  (when the mirror is fixed). We find that when the difference between the atomic frequency  $\omega_a$  and the cavity frequency  $\omega_0$  is larger than 25, there is no steady-state near the detuning  $\Delta_c$ . When  $-0.95 \lesssim \Delta_0 \lesssim 25$ , there are two steady-state solutions, i.e.,  $\Delta_{p,s}^{(1)}$  and  $\Delta_{p,s}^{(2)}$  shown in Fig. 3. In this region, we find that  $\Delta_{p,s}^{(1)}$  decreases linearly, but  $\Delta_{p,s}^{(2)}$  increases with increasing  $\Delta_0$ . When  $\Delta_0 \lesssim -0.95$ , as shown in Fig. 3, there are four steady-state solutions, i.e.,  $\Delta_{p,s}^{(i)}$  ( $i = 1, 2, 3, 4$ ). Figure 3 shows that when the detuning  $\Delta_0$  passes through  $-0.95$ , from the right to the left, two additional solutions ( $\Delta_{p,s}^{(3)}$  and  $\Delta_{p,s}^{(4)}$ ) appear. We also find that two solutions ( $\Delta_{p,s}^{(2)}$  and  $\Delta_{p,s}^{(4)}$ ) gradually approach  $\Delta_c = 0$  to realize the

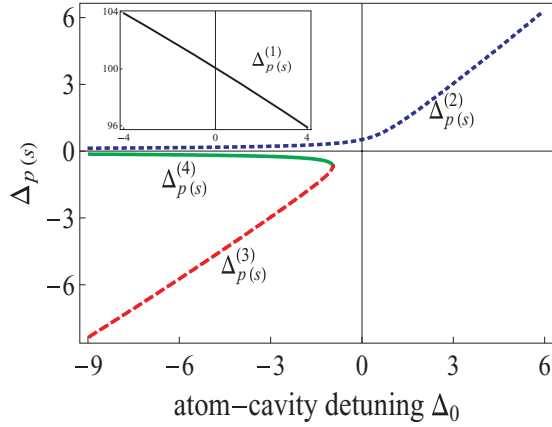


FIG. 3. (Color online) The steady-state solutions  $\Delta_{p,s}^{(i)}$  ( $i = 1, 2, 3, 4$ ) versus the atom-cavity detunings  $\Delta_0$  (when the two mirrors are fixed) for given parameters, e.g.,  $\kappa = 10^2$ ,  $\Delta_c = 0$ ,  $\omega_a = 10^6$ ,  $\gamma_0 = 10^{-6}$ ,  $\gamma_2 = 10^{-4}$ ,  $g = 10^2$ ,  $\Omega = 2$ , and  $a_{in} = 10$ . Hereafter, all the quantities are measured in units of  $\gamma_1$ . Note that here eight parameters determine the system. Recall that  $\Delta_{p,s}$  is the steady-state atom-cavity detuning when one mirror is movable. The inset shows the steady-state solution  $\Delta_{p,s}^{(1)}$ , which corresponds to a very large displacement of the mirror. As schematically shown in Fig. 2(b), the dotted blue, dashed red, and continuous green lines denote the solutions  $\Delta_{p,s}^{(2)}$ ,  $\Delta_{p,s}^{(3)}$ , and  $\Delta_{p,s}^{(4)}$ , respectively. For example, the green cross in Fig. 2(b) corresponds to a single value of  $\Delta_0$ . Here,  $\Delta_0$  is swept, and the green cross in Fig. 2(b) becomes a continuous curve. Same for one red dot and one blue square in Fig. 2(b).

two-photon-resonance condition. Moreover, note that  $\Delta_{p,s}^{(3)}$  increases almost linearly with increasing  $\Delta_0$ .

With the same parameters as those in Fig. 3, we have also plotted in Fig. 4 the  $\Delta_0$ -dependent location  $\langle x \rangle_s^{(i)}$  of the mirror corresponding to  $\Delta_{p,s}^{(i)}$ . We find that there is no solution for the steady-state value of  $\langle x \rangle_s^{(i)}$  when  $\Delta_0 \gtrsim 25$ . When  $-0.95 \lesssim \Delta_0 \lesssim 25$ , the mirror's position  $\langle x \rangle_s^{(1)}$ , corresponding to the solution  $\Delta_{p,s}^{(1)}$ , exhibits a very large (compared with  $\langle x \rangle_s^{(2)}$ ,

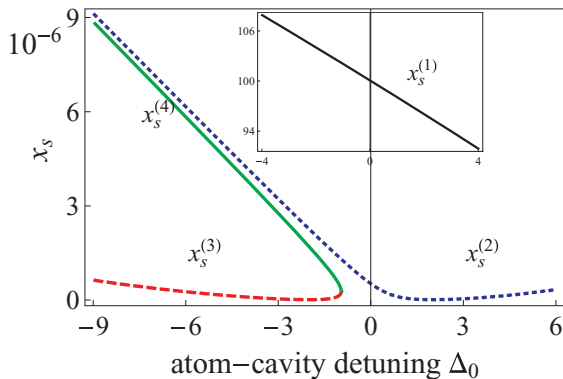


FIG. 4. (Color online) Steady-state positions  $\langle x \rangle_s^{(i)}$  ( $i = 1, 2, 3, 4$ ) for the movable mirror versus the atom-cavity detuning  $\Delta_0$ , for the same parameters listed in Fig. 3. Here, the continuous black, dotted blue, dashed red, continuous green lines denote  $\langle x \rangle_s^{(1)}$ ,  $\langle x \rangle_s^{(2)}$ ,  $\langle x \rangle_s^{(3)}$ , and  $\langle x \rangle_s^{(4)}$ , when the atom-cavity detunings  $\Delta_{p,s}$  take the following steady-state values  $\Delta_{p,s}^{(1)}$ ,  $\Delta_{p,s}^{(2)}$ ,  $\Delta_{p,s}^{(3)}$ , and  $\Delta_{p,s}^{(4)}$ , respectively, as shown in Fig. 3.

$\langle x \rangle_s^{(3)}$ ,  $\langle x \rangle_s^{(4)}$ ) displacement of the mirror, and  $\langle x \rangle_s^{(1)}$  increases as  $\Delta_0$  increases. The mirror's displacement  $\langle x \rangle_s^{(2)}$ , corresponding to the solution  $\Delta_{p,s}^{(2)}$ , is nearly zero. When  $\Delta_0 \lesssim -0.95$ , the four steady-state solutions for the displacement  $\langle x \rangle_s$  exist simultaneously. Two of them,  $\langle x \rangle_s^{(2)}$  and  $\langle x \rangle_s^{(4)}$ , show that the spring is compressed, and their displacements linearly increase when  $\Delta_0$  decreases. One of them,  $\langle x \rangle_s^{(3)}$ , nearly vanishes.

From Eq. (19), we know that the oscillating mirror can affect the two-photon resonance by changing the effective frequency  $\omega_L$  of the cavity field. Because when the mirror is fixed, the two-photon resonant condition becomes

$$\Delta_0 = \omega_a - \omega_0 = \Delta_c. \quad (34)$$

However, this condition is modified to

$$\Delta_{p,s} = \omega_a - \omega_L = \Delta_c, \quad (35)$$

when the mirror is oscillating. We note that the two-photon resonant condition in Eq. (35) is further modified to

$$\Delta_{p,s}^{(i)} = \omega_a - \omega_L = \Delta_c, \quad (36)$$

when the system reaches its steady state. We assume that the two-photon resonant condition in Eq. (34) is satisfied when the mirror is fixed. Recall that  $\Delta_c = 0$  in Figs. 3 and 4. This means that the two-photon resonant condition is  $\Delta_{p,s}^{(i)} = 0$  in this case. We find that  $\langle x \rangle_s$  is nearly zero as shown in Fig. 4 when  $\Delta_0 > \Delta_c = 0$ . In this case, there is no value of  $\Delta_{p,s}$  approaching zero, as shown in Fig. 3; so the two-photon resonance cannot happen. From Figs. 3 and 4, we find that the two-photon resonance  $\Delta_{p,s}^{(i)} = \Delta_c = 0$  might happen when  $\Delta_0 \lesssim -0.95$ . Because in this region,  $\Delta_{p,s}^{(2)}$  and  $\Delta_{p,s}^{(4)}$  can approach zero as in Fig. 3, which correspond to the steady-state values of the mirror's positions  $\langle x \rangle_s^{(2)}$  and  $\langle x \rangle_s^{(4)}$ , respectively, as in Fig. 4.

We now turn to study the steady-state values of  $\Delta_{p,s}$  and  $\langle x \rangle_s$  for the case when  $6400 \lesssim \kappa < \infty$ , e.g.,  $\kappa = 10^4$ . In this case, as schematically shown in Fig. 2(b), there are three critical values  $\Delta_{th}^{(i)}$  ( $i = ab, bc, cd$ ):  $\Delta_{th}^{(cd)} \cong 2.5 \times 10^3$ ,  $\Delta_{th}^{(bc)} \cong -0.22$  and  $\Delta_{th}^{(ab)} \cong -2.5 \times 10^5$ . The number of solutions for  $\Delta_{p,s}$  has the same descriptions as those in Fig. 2(b). Similarly to Figs. 3 and 4, we plot Figs. 5 and 6 for  $\Delta_{p,s}^{(i)}$  and their corresponding  $\langle x \rangle_s^{(i)}$ , respectively. The two-photon resonance condition in Eq. (36) for  $\Delta_c = 0$  might also be satisfied in this case. Because when  $\Delta_0 \lesssim -0.22$ , two steady-state values ( $\Delta_{p,s}^{(2)}$  and  $\Delta_{p,s}^{(4)}$ ) of  $\Delta_{p,s}$  are near zero, as shown in Fig. 5, which correspond to the steady-state solution of the mirror's position  $\langle x \rangle_s^{(2)}$  and  $\langle x \rangle_s^{(4)}$ , as shown in Fig. 6. It is also found that one,  $\langle x \rangle_s^{(2)}$ , of the steady-state solutions of  $\langle x \rangle_s$  nearly vanishes, as shown in Fig. 6, when  $\Delta_0 > \Delta_c = 0$ .

Finally, we note that there is only one steady state solution  $\Delta_{p,s} = \Delta_0$  for Eq. (28) in the limit  $\kappa \rightarrow \infty$ . This implies when the elastic coefficient  $M\omega_M^2$  is very large for given cavity length  $l$ , it is difficult for the photon pressure to make the mirror to even have a tiny displacement, and the oscillating mirror does not affect the optomechanical system [30].

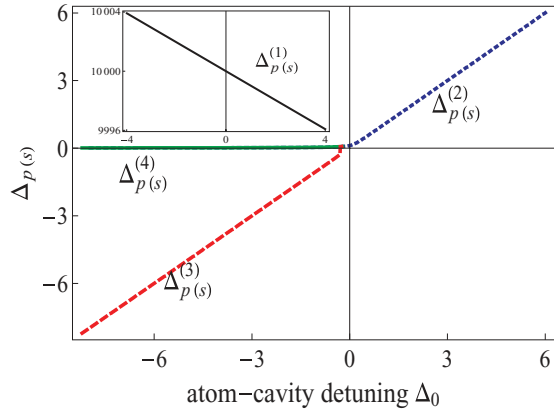


FIG. 5. (Color online) Steady-state solutions  $\Delta_{p(s)}^{(i)}$  ( $i = 1, 2, 3, 4$ ) schematically shown in Fig. 2(b) versus  $\Delta_0$  with  $\kappa = 10^4$ . The other parameters here are the same as in Fig. 3. The inset shows the steady state solution  $\Delta_{p(s)}^{(1)}$  that corresponds to a very large displacement of the mirror. As shown in Fig. 2(b), the dotted blue, dashed red, and continuous green lines denote the solutions  $\Delta_{p(s)}^{(2)}$ ,  $\Delta_{p(s)}^{(3)}$ , and  $\Delta_{p(s)}^{(4)}$ , respectively.

#### IV. ELECTROMAGNETICALLY INDUCED TRANSPARENCY IN THE OPTOMECHANICAL SYSTEM

To explore how the mirror's oscillation affects the EIT, let us now study the susceptibility of the atomic medium. Because we can write the probe cavity field as

$$E(t) = \sqrt{\frac{\omega L}{2V\epsilon_0}} a e^{-i\omega_L t} + \text{H.c.} = \epsilon e^{-i\omega_L t} + \text{H.c.}, \quad (37)$$

then the linear response of the atomic ensemble to the weak probe field  $E(t)$  can be described by the susceptibility

$$\chi = \frac{\langle p \rangle}{\langle \epsilon \rangle \epsilon_0}. \quad (38)$$

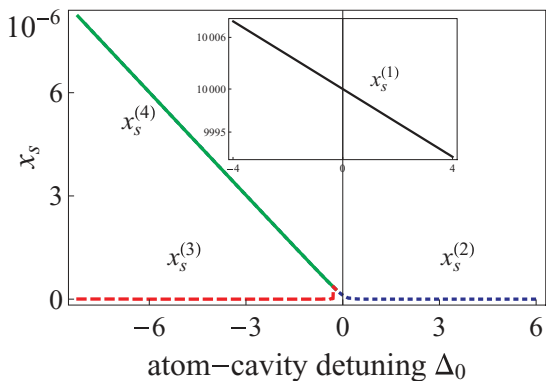


FIG. 6. (Color online) Steady-positions  $\langle x_s^{(i)} \rangle$  ( $i = 1, 2, 3, 4$ ) of the movable mirror versus the atom-cavity detuning  $\Delta_0$ , with the same parameters as in Fig. 5. Here, the continuous black, dotted blue, dashed red, continuous green lines denote  $\langle x_s^{(1)} \rangle$ ,  $\langle x_s^{(2)} \rangle$ ,  $\langle x_s^{(3)} \rangle$ , and  $\langle x_s^{(4)} \rangle$ , when the atom-cavity detunings  $\Delta_{p(s)}$  (for a moving mirror) takes the following steady-state values:  $\Delta_{p(s)}^{(1)}$ ,  $\Delta_{p(s)}^{(2)}$ ,  $\Delta_{p(s)}^{(3)}$ , and  $\Delta_{p(s)}^{(4)}$ , respectively, as shown in Fig. 5.

Here, the average polarization  $\langle p \rangle$  of the atomic ensemble is

$$\langle p \rangle = \frac{\mu}{V} \sum_{i=1}^N \sigma_{ba}^{(i)}. \quad (39)$$

Using Eqs. (24), (37), and (38), we obtain the susceptibility  $\chi$

$$\chi = F \frac{\gamma_2 \Xi - (\Delta_{p,s} - \Delta_c) \Theta}{\Xi^2 + \Theta^2} + i F \frac{\gamma_2 \Theta + (\Delta_{p,s} - \Delta_c) \Xi}{\Xi^2 + \Theta^2}, \quad (40)$$

with

$$F = \frac{\mu^2 N}{\epsilon_0 V}, \quad (41)$$

$$\Xi = \gamma_1 (\Delta_{p,s} - \Delta_c) + \gamma_2 \Delta_{p,s}, \quad (42)$$

(where  $F$  is proportional to the density  $N/V$ ) and

$$\Theta = \Omega^2 - \Delta_{p,s} (\Delta_{p,s} - \Delta_c) + \gamma_1 \gamma_2. \quad (43)$$

It is well known that the real part,  $\text{Re}(\chi)$ , and the imaginary part,  $\text{Im}(\chi)$ , of the susceptibility  $\chi$  describe the dispersion and absorption of light, respectively.

As discussed in the last section, one of the solutions corresponding to  $x_s^{(1)}$  and  $\Delta_{p,s}^{(1)}$  is unstable, and another solution, corresponding to  $x_s^{(4)}$  and  $\Delta_{p,s}^{(4)}$ , is similar to the solution  $x_s^{(2)}$  and  $\Delta_{p,s}^{(2)}$  in the region  $(\Delta_{th}^{(b)}, \Delta_{th}^{(c)})$ . Therefore, we only consider two solutions below. In Fig. 7,  $\text{Re}(\chi_i)$  and  $\text{Im}(\chi_i)$  ( $i = 1, 2$ ) versus  $\Delta_0$  are plotted for the two solutions  $\Delta_{p,s}^{(2)}$  and  $\Delta_{p,s}^{(3)}$  studied in Fig. 3. Here,  $\chi_1$  and  $\chi_2$  denote the susceptibilities corresponding to  $\Delta_{p,s}^{(2)}$  and  $\Delta_{p,s}^{(3)}$ , respectively. All parameters in Fig. 7 are the same as those in Fig. 3. It is found that when  $\Delta_0 > \Delta_c = 0$ , the curves for  $\text{Re}(\chi_1)$  and  $\text{Im}(\chi_1)$  are similar to those in the usual EIT phenomenon [30]. This means that the steady-state value  $\langle x_s^{(2)} \rangle$  of the mirror's

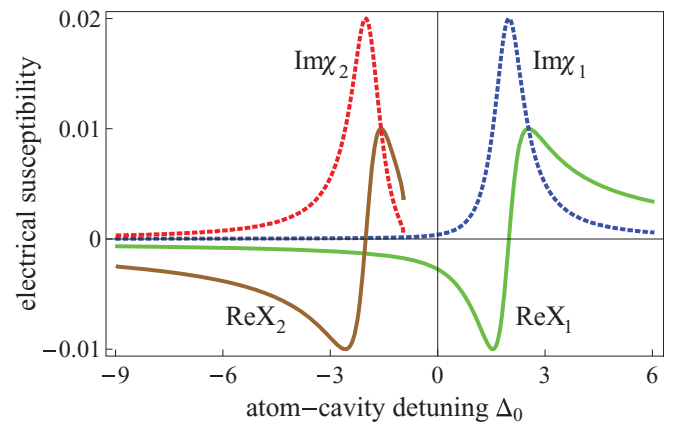


FIG. 7. (Color online) The susceptibilities  $\chi_1$  and  $\chi_2$  for the detuning between the atom and the control field  $\Delta_c = 0$  and  $\kappa = 10^2$ . We plot only two susceptibilities because there are three stable solutions in this parameter region but two of them are quite similar. Here, the dotted and solid curves correspond to the imaginary and real parts, respectively. The blue and the green colors correspond to  $\chi_1$  and the dark red and brown colors correspond to  $\chi_2$ , respectively. The EIT-like region is located between the two peaks of  $\text{Im}\chi_1$  and  $\text{Im}\chi_2$ .

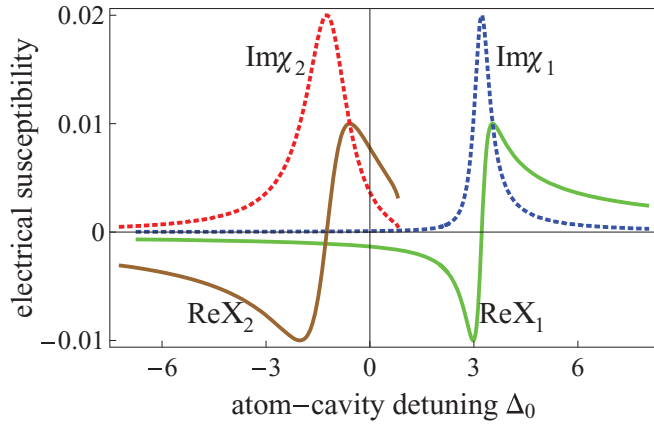


FIG. 8. (Color online) The susceptibilities  $\chi_1$  and  $\chi_2$  for  $\Delta_c = 2$  and  $\kappa = 10^2$ . Here, the dotted and solid curves correspond to the imaginary and real parts, respectively. The blue and the green colors correspond to  $\chi_1$  and the dark red and brown colors correspond to  $\chi_2$ , respectively. The EIT-like region is located between the two peaks of  $\text{Im}\chi_1$  and  $\text{Im}\chi_2$ .

displacement is near zero in this region of parameters, and the oscillating mirror has no effect on the EIT. However, when  $\Delta_0 < \Delta_c = 0$ , the mirror's displacement  $\langle x \rangle_s^{(2)}$  makes the two-photon-resonance condition  $\Delta_{p,s}^{(2)} = \omega_a - \omega_L \approx \Delta_c = 0$  approximately satisfied. As a result, in this region, each of the curves  $\text{Re}(\chi_i)$  and  $\text{Im}(\chi_i)$  is almost close to zero, like an infinite "tail." When  $\Delta_0 \lesssim -0.95$  as shown in Fig. 3, another

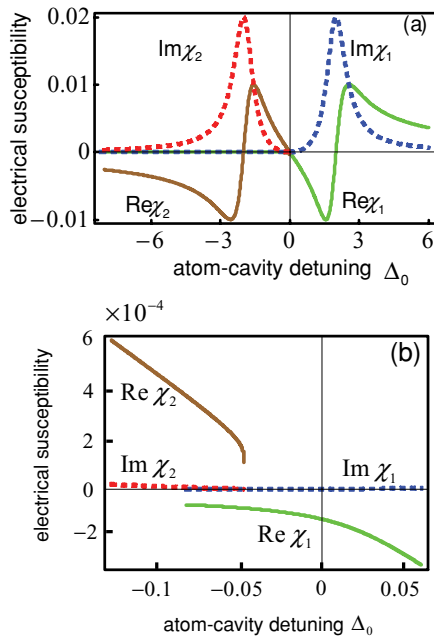


FIG. 9. (Color online) (a) The susceptibilities  $\chi_1$  and  $\chi_2$  for  $7\Delta_c = 0$  and  $\kappa = 10^6$ . (b) The magnified figure of (a) for small  $\Delta_0$ . Here, the dotted and solid curves correspond to the imaginary and real parts, respectively. The blue and the green colors correspond to  $\chi_1$  and the dark red and brown colors correspond to  $\chi_2$ , respectively. It is shown in these two figures that the oscillating mirror's influence on EIT can also be observed if the detector's resolving power is high enough.

solution  $\Delta_{p,s}^{(3)}$  emerges, thus we also have a  $\Delta_{p,s}^{(3)}$ -dependent susceptibility  $\chi_2$ .

As shown in Fig. 7, the curves corresponding to the real part  $\text{Re}(\chi_2)$  and the imaginary part  $\text{Im}(\chi_2)$  of the susceptibility  $\chi_2$  are similar to those in the usual EIT [30], since the mirror's displacement  $\langle x \rangle_s^{(3)}$  is nearly zero. From Fig. 7, we find that the right part of the curve  $\text{Im}(\chi_2)$  almost merges with the left part of the curve  $\text{Im}\chi_1$ , so that a transparent "window" is formed.

To know how  $\Delta_c$  affects the EIT, we can also study the susceptibility  $\chi$  for the detuning  $\Delta_c = 2$  when other parameters are assumed to be the same as those in Fig. 7. As shown in Fig. 8, the steady-state solutions of  $\Delta_{p,s}$  and  $\langle x \rangle_s$  are similar to those for  $\Delta_c = 0$ . The curves corresponding to these solutions are just rightward shifts for the curves in Figs. 3 and 4, but the shapes of the curves are almost the same. Similar to Fig. 7, we choose two steady-state solutions and plot  $\text{Re}(\chi_i)$  and  $\text{Im}(\chi_i)$  ( $i = 1, 2$ ) versus  $\Delta_0$ . Obviously, the essential conclusions remain unchanged as those in Fig. 7, but all curves have a rightward shift.

Based on the analysis in Sec. III,  $\Delta_{\text{th}}^{(bc)}$  and  $\Delta_{\text{th}}^{(ab)}$  approach zero from the left side when  $\kappa$  is increased. When  $\kappa > \kappa_L$ , e.g.,  $\kappa \gtrsim 6400$  in Figs. 5 and 6, the larger  $\kappa$  corresponds to shorter "tails" of the curves corresponding to  $\text{Re}(\chi_1)$  and  $\text{Im}(\chi_1)$  when  $\Delta_0 \gtrsim -0.95$ . As shown in Figs. 9(a) and 9(b), for the parameters in the current experiments [7,8], such as  $\kappa \sim 10^6$  discussed as above, the "tails" phenomenon can be detected if the resolution of the detector is high enough. Actually, a small elastic constant can be obtained in optomechanical systems formed by a quantum-degenerate Fermi gas [37], where the mechanical motion of the fermionic particle-hole

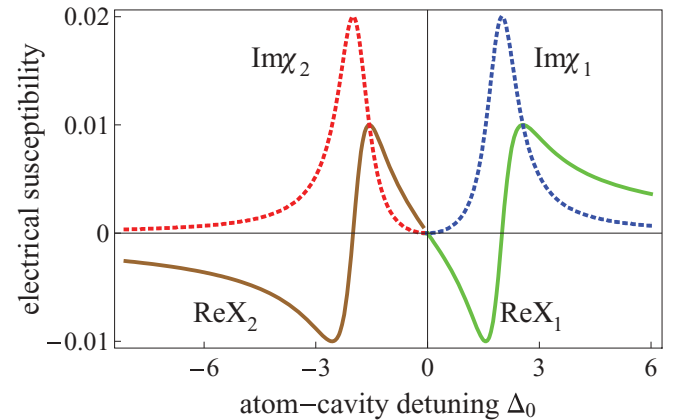


FIG. 10. (Color online) The susceptibilities for  $\Delta_c = 0$  and  $\kappa = 1.6 \times 10^{10}$ . Note that this value of the elastic constant  $\kappa$  is huge, corresponding to an almost fixed mirror. In this case, the  $\text{Re}\chi_1$  and  $\text{Im}\chi_1$  occur for mostly positive values of the atom-cavity detuning. When the spring constant becomes softer, as in Fig. 7, the  $\text{Re}\chi_1$  and  $\text{Im}\chi_1$  have a response that extend over a huge range of values of the atom-cavity detuning  $\Delta_0$ , even for  $\Delta_c \gtrsim -6$ . When  $\kappa$  tends to infinity, the susceptibility becomes the same as that in the usual EIT phenomenon. This consistency check is reassuring for our calculations. Here, the dotted and solid curves correspond to the imaginary and real parts, respectively. The blue and the green colors correspond to  $\chi_1$  and the dark red and brown colors correspond to  $\chi_2$ , respectively. The EIT-like region occurs near zero detuning  $\Delta_0$ .

system behaves as a “moving mirror.” The frequency of the oscillating “mirror” is about 0.1 MHz. We hope that the above discussed physical effects for the small elastic constant can be first observed in such system [37] or other condensed matter systems. For the real optomechanical systems, the frequency of the mirror can reach  $0.5 \sim 2$  MHz [38,39] with the cavity length (100 nm) [40].

In the limit  $\kappa \rightarrow \infty$ , the “tails” (for  $\Delta_0 \gtrsim 0$ ) disappear and the right part of the curve  $\text{Im}(\chi_2)$  just meets the left part of the curve  $\text{Im}(\chi_1)$  to form a transparent “window.” In this limit, all the physical properties return to that in the usual EIT phenomenon. Namely, we recover the standard EIT when  $\kappa \rightarrow \infty$ . This asymptotic result is shown in Fig. 10 with a large  $\kappa$  (e.g.,  $\kappa = 1.6 \times 10^{10}$ ), but other parameters are the same as in Fig. 3. In Fig. 10, around the point  $\Delta_0 > \Delta_c = 0$ , the left parts of the curves  $\text{Re}(\chi_1)$  and  $\text{Im}(\chi_1)$  nearly merge with the right parts of the curves  $\text{Re}(\chi_2)$  and  $\text{Im}(\chi_2)$ , and thus transparent windows are formed as in the usual EIT [30].

## V. CONCLUSION AND REMARKS

We have studied the effects of the end mirror’s oscillation on the EIT phenomenon for an atomic ensemble confined in a gas cell placed in a microcavity. This study can help us to quantitatively consider the quantum interface between an optomechanical system and an atomic gas displaying EIT. The results obtained could be used to improve the measurement precision based on the EIT effect, when the medium is placed

inside a microcavity with a one-end oscillating mirror and the cavity acts as the probe light. We have shown that the whole system exhibits multistability due to the mirror’s vibration, and we have also numerically obtained the threshold values of the parameters, which can help determine how many steady states exist in the corresponding parameter regions. This multistability can be explicitly displayed through a modified EIT phenomenon. Consequently, we investigate the effects of the multi-steady-state solutions on the EIT phenomenon and find that in some parameter regions there are two solutions that approximately satisfy the two-photon resonance condition. Therefore, the properties of both the real and imaginary parts of the susceptibility are significantly altered. When the spring elastic constant increases, the mirror becomes less movable, our study show that in this case all properties of the system gradually revert to those of the usual EIT phenomenon.

## ACKNOWLEDGMENTS

C.P.S. acknowledges supports by the NSFC with Grants No. 10474104, No. 60433050, and No. 10704023, NFRPC Nos. 2006CB921205 and 2005CB724508. Y.X.L. acknowledges supports by the NSFC with Grants No. 10975080 and 61025022. F.N. was supported in part by the National Security Agency (NSA), the Laboratory for Physical Sciences (LPS), the Army Research Office (ARO), the National Science Foundation (NSF) Grant No. EIA-0130383, and the JSPS-RFBR 06-02-91200.

- 
- [1] S. Mancini and P. Tombesi, *Phys. Rev. A* **49**, 4055 (1994).
  - [2] D. Meiser and P. Meystre, *Phys. Rev. A* **73**, 033417 (2006).
  - [3] D. Vitali, S. Gigan, A. Ferreira, H. R. Böhm, P. Tombesi, A. Guerreiro, V. Vedral, A. Zeilinger, and M. Aspelmeyer, *Phys. Rev. Lett.* **98**, 030405 (2007).
  - [4] W. Marshall, C. Simon, R. Penrose, and D. Bouwmeester, *Phys. Rev. Lett.* **91**, 130401 (2003).
  - [5] S. Mancini, D. Vitali, and P. Tombesi, *Phys. Rev. Lett.* **80**, 688 (1998).
  - [6] C. Genes, D. Vitali, P. Tombesi, S. Gigan, and M. Aspelmeyer, *Phys. Rev. A* **77**, 033804 (2008).
  - [7] M. Bhattacharya and P. Meystre, *Phys. Rev. Lett.* **99**, 073601 (2007).
  - [8] M. Bhattacharya, H. Uys, and P. Meystre, *Phys. Rev. A* **77**, 033819 (2008).
  - [9] M. Bhattacharya, P.-L. Giscard, and P. Meystre, *Phys. Rev. A* **77**, 030303 (2008).
  - [10] M. Bhattacharya and P. Meystre, *Phys. Rev. A* **78**, 041801 (2008).
  - [11] J. Q. You and F. Nori, *Phys. Rev. B* **68**, 064509 (2003).
  - [12] A. Wallraff, D. I. Schuster, A. Blais, L. Frunzio, R.-S. Huang, J. Majer, S. Kumar, S. M. Girvin, and R. J. Schoelkopf, *Nature (London)* **431**, 162 (2004).
  - [13] J. Q. You and F. Nori, *Phys. Today* **58**(11), 42 (2005).
  - [14] F. Nori, *Nat. Phys.* **4**, 589 (2008).
  - [15] Y. X. Liu, L. F. Wei, J. R. Johansson, J. S. Tsai, and F. Nori, *Phys. Rev. B* **76**, 144518 (2007).
  - [16] S. Kleff, S. Kehrein, and J. von Delft, *Phys. Rev. B* **70**, 014516 (2004).
  - [17] P. R. Berman, *Cavity Quantum Electrodynamics* (Academic Press, New York, 1994).
  - [18] C. Genes, D. Vitali, and P. Tombesi, *Phys. Rev. A* **77**, 050307 (2008).
  - [19] H. Ian, Z. R. Gong, Y. X. Liu, C. P. Sun, and F. Nori, *Phys. Rev. A* **78**, 013824 (2008).
  - [20] S. E. Harris, *Phys. Today* **50**(7), 36 (1997).
  - [21] M. Fleischhauer and A. S. Manka, *Phys. Rev. A* **54**, 794 (1996).
  - [22] L. V. Hau, S. E. Harris, Z. Dutton, and C. H. Behroozi, *Nature (London)* **397**, 594 (1999).
  - [23] M. Fleischhauer and M. D. Lukin, *Phys. Rev. Lett.* **84**, 5094 (2000).
  - [24] M. O. Scully and M. S. Zubairy, *Quantum Optics* (Cambridge University Press, Cambridge, 1997).
  - [25] C. P. Sun, Y. Li, and X. F. Liu, *Phys. Rev. Lett.* **91**, 147903 (2003).
  - [26] M. D. Lukin, *Rev. Mod. Phys.* **75**, 457 (2003).
  - [27] O. Kocharovskaya, Y. Rostovtsev, and M. O. Scully, *Phys. Rev. Lett.* **86**, 628 (2001).
  - [28] L. Deng, E. W. Hagley, M. Kozuma, and M. G. Payne, *Phys. Rev. A* **65**, 051805(R) (2002).
  - [29] M. Kozuma, D. Akamatsu, L. Deng, E. W. Hagley, and M. G. Payne, *Phys. Rev. A* **66**, 031801(R) (2002).
  - [30] Y. Li and C. P. Sun, *Phys. Rev. A* **69**, 051802(R) (2004).

- [31] L. He, Y. X. Liu, S. Yi, C. P. Sun, and F. Nori, *Phys. Rev. A* **75**, 063818 (2007).
- [32] Z. R. Gong, H. Ian, L. Zhou, and C. P. Sun, *Phys. Rev. A* **78**, 053806 (2008).
- [33] M. D. Lukin, S. F. Yelin, and M. Fleischhauer, *Phys. Rev. Lett.* **84**, 4232 (2000).
- [34] M. Fleischhauer and M. D. Lukin, *Phys. Rev. A* **65**, 022314 (2002).
- [35] Y. Chang, H. Ian, and C. P. Sun, *J. Phys. B* **42**, 215502 (2009).
- [36] M. L. Bellac, *Quantum and Statistical Field Theory* (Oxford University Press, Oxford, 1992).
- [37] R. Kanamoto and P. Meystre, *Phys. Rev. Lett.* **104**, 063601 (2010).
- [38] A. Nunnenkamp, K. Borkje, J. G. E. Harris, and S. M. Girvin, *Phys. Rev. A* **82**, 021806(R) (2010).
- [39] O. R. Isart, A. C. Pflanzer, M. L. Juan, R. Quidant, N. Kiesel, M. Aspelmeyer, and J. I. Cirac, *Phys. Rev. A* **83**, 013803 (2011).
- [40] S. Singh, G. A. Phelps, D. S. Goldbaum, E. M. Wright, and P. Meystre, *Phys. Rev. Lett.* **105**, 213602 (2010).